LAWRENCE
LIVERMORE
NATIONAL
LABORATORY

UCRL-JRNL-211347

Anisotropy of electrical conductivity in dry olivine

W. L. Du Frane, J. J. Roberts, D. A. Toffelmier, J. A. Tyburczy

April 13, 2005

Geophysical Research Letters

UCRL-JRNL-211347

Anisotropy of electrical conductivity in dry olivine

Wyatt L. Du Frane[1,2], Jeffery J. Roberts[2], Daniel A. Toffelmier[1], James A. Tyburczy[1]

[1] Department of Geological Sciences, Arizona State University, Tempe, Arizona, USA
[2] Experimental Geophysics Group, Lawrence Livermore National Laboratory, Livermore, California, USA

[1] The electrical conductivity (σ) was measured for a single crystal of San Carlos olivine ($Fo_{89.1}$) for all three principal orientations over oxygen fugacities $10^{-7}<fO_2<10^{1}$ Pa at 1100, 1200, and 1300ºC. Fe-doped Pt electrodes were used in conjunction with a conservative range of fO_2, T, and time to reduce Fe loss resulting in data that is ~0.15 log units higher in conductivity than previous studies. At 1200ºC and $fO_2=10^{-1}$ Pa, $\sigma_{[100]}=10^{-2.27}$S/m, $\sigma_{[010]}=10^{-2.49}$S/m, $\sigma_{[001]} = 10^{-2.40}$S/m. The dependences of σ on T and fO_2 have been simultaneously modeled with undifferentiated mixed conduction of small polarons and Mg vacancies to obtain steady-state fO_2-independent activation energies: $Ea_{[100]}$ = 0.32 eV, $Ea_{[010]}$ = 0.56 eV, $Ea_{[001]}$ = 0.71 eV. A single crystal of dry olivine would provide a maximum of $\sim10^{0.4}$ S/m azimuthal σ contrast for T<1500ºC. The anisotropic results are combined to create an isotropic model with Ea = 0.53 eV.

INTRODUCTION

[2] Electrical anisotropy has been reported synonymously with seismic anisotropy and high mantle electrical conductivity (σ) beneath mid-ocean ridges, subduction zones, and cratons [*Simpson*, 2002; *Eaton et al.*, 2004; *Evans et al.*, 2005]. Magnetotelluric (MT) results suggests that mantle electrical anisotropy factors range from 2-100 [*Simpson*, 2002; *Evans et al.*, 2005] potentially as a result of deformation-induced orientation of minerals. Anisotropy factors of naturally sheared peridotites can be determined using single-crystal olivine measurements and resistor network modeling [*e.g. Simpson and Tommasi*, 2005]. Electrical properties of minerals are highly sensitive to factors such as orientation, oxygen fugacity (fO_2), Fe content, water (H^+) content, and temperature (T); these factors require careful laboratory investigation to further our interpretation of the recent mantle anisotropy observations by MT. Electrical properties are often complementary to seismic properties; they are very sensitive to water fugacity [*Huang et al.*, 2005], and they can be useful in determining mantle geotherms [*Shankland and Duba*, 1990].

[3] We have collected a unique set of σ data over fO_2-T space for three orientations of a dry single crystal of San Carlos olivine (SCO) and use a defect model of the data to address the possible causes of observed mantle electrical anisotropy. fO_2 is not well known in the mantle, but is constrained by mineral oxygen buffer assemblages. The effects of nonlinear fO_2 dependence are examined at 1100, 1200, and 1300ºC. The T dependent SO1 [*Shankland and Duba*, 1990] and SO2 [*Constable et al.*, 1992] models are based on an σ dataset of single crystal SCO ($Fo_{91.7}$) for each principal orientation, using Ir electrodes, a constant $7CO_2$:1CO gas mixture, and a constant heating rate of 1ºC/min. Determination of σ and apparent activation energies (Ea) by this method has slight kinetic problems because the samples are not fully equilibrated with the effects of changing fO_2 and T [*Shankland and Duba*, 1990; *Wanamaker and Duba,* 1993]. *Wanamaker and Duba* [1993] determined the fO_2 and T dependence of SCO σ in the [100] direction in fully equilibrated experiments. We present fully equilibrated data for the [100], [010], and [001] directions, modeled for the separate dependences of fO_2 and T, using mixed conduction of small polarons (Fe^{3+} in octahedral Mg sites; written as $Fe^{\bullet}_{Mg}$) and magnesium vacancies (written as V''_{Mg}) to obtain steady-state, fO_2-independent Ea for each principal orientation of olivine. We provide anisotropic and isotropic olivine models useful for interpreting MT data.

EXPERIMENTAL TECHNIQUES

[4] A single crystal of SCO was determined by electron microprobe analysis (EMPA) to be $Fo_{89.1}$, oriented using back-reflection Laue x-ray diffraction and cut into four samples (~0.5 x 3 x 3 mm) within 5 degrees of each principal axis from the crystal: SCC2_100B, SCC2_010A, SCC2_001A, and SCC2_001B. The second [001] oriented sample was cut to determine the repeatability of the measurements and to aid modeling.

[5] One problem in measuring σ of olivine has been experimental iron loss to the electrodes, resulting in a reduced population of small polarons. Iridium electrodes have been used in place of Pt to help reduce Fe loss [*Schock et al.*, 1989; *Wanamaker and Duba*, 1993]. Fe-doped Pt electrodes [*Grove*, 1981] allowed us to conduct these experiments with only minor Fe loss, confirmed by EMPA. The electrode material was prepared by filling a Pt capsule with a mixture of 95% olivine $(Fe_{0.20}Mg_{0.80})_2SiO_4$ and 5% basalt (TT-152 MORB) and firing it in an internally heated pressure vessel for 5 days at 1126 to 1200ºC and 400 MPa pressure. EMPA of a cross-section of the foil (0.25mm thick) indicated a gradient of Fe in the Pt capsule wall from 6 wt% on the sample side to ~0 wt% at the center of the capsule wall.

[6] Measurements were made in 1-atm gas mixing furnaces [*Netherton and Duba*, 1978]. σ measurements were made with an LCR meter (HP4284a). Data reported here were measured with a 500-mV 1-kHz AC signal, which was determined through impedance spectroscopy to exclude the inductive and capacitive effects of our system on the overall sample impedance measurement [*Roberts and Tyburczy*, 1991, 1993]. fO_2 was controlled using a CO_2:CO mixture and measured by an Y-stabilized zirconia sensor. All conductivity data points were measured after samples equilibrated to new T and fO_2 conditions for a minimum of 5 hours. Irreversible Fe exchange was avoided by not allowing samples to equilibrate with their electrodes and maintaining an fO_2 range where Fe loss is minimal and limiting temperature to 1300˚C.

DATA ANALYSIS AND RESULTS

[7] σ data, along with our fits, are shown for each sample at each T in Figure 1. For comparison of our raw σ measurements we normalize previous σ measurements to account for differences in Fe content [*Hirsch et al.*, 1993]. As a result of less Fe loss (verified by EMPA) through the use of Fe-doped electrodes and conservative experimental conditions, our data fits of single-crystal San Carlos olivine are on average 0.14 and 0.17 log units higher than σ by *Schock et al.* [1989] and *Wanamaker and Duba* [1993], respectively (Figure 1b). The two [001] oriented samples show our σ measurements are repeatable to ~0.05 log units. At 1100ºC, $\sigma_{[100]}$ and $\sigma_{[001]}$ are similar in magnitude and are both greater than $\sigma_{[010]}$. For 1200ºC, we generally see that $\sigma_{[010]} < \sigma_{[100]} < \sigma_{[001]}$, consistent with *Schock et al.* [1989]. At 1300ºC, $\sigma_{[100]}$ and $\sigma_{[010]}$ are similar and $10^{0.1}$ S/m lower than $\sigma_{[001]}$. For all samples σ increases with fO_2 and T.

[8] The relationship describing the major defect populations and their fO_2 dependences of olivine [*Stocker and Smyth*, 1978, *Schock et al.*, 1989] is:

$$8Fe_{Mg}^{x} + 2O_2 \Leftrightarrow 2V_{Mg}^{''} + V_{Si}^{''''} + 4O_o^x + 8Fe_{Mg}^{\bullet}, \quad (1)$$

where $V_{Si}^{''''}$ is a silicon vacancy, Fe_{Mg}^{x} is an octahedral site containing Fe^{2+} ions, and O_o^x is an oxygen site containing an O^{2-} ion. For a fixed cationic ratio and high fO_2, we have the charge balance condition $4[V_{Mg}^{''}] = [Fe_{Mg}^{\bullet}] = 8[V''''_{Si}]$ [*Stocker*, 1978] for Equation 1 that yields:

$$[Fe_{Mg}^{\bullet}] = a_{Fe} fO_2^{2/11}, \quad (2)$$

$$[V_{Mg}^{''}] = a_{Mg} fO_2^{2/11}, \quad (3)$$

where $[Fe_{Mg}^{\bullet}]$ is small polaron concentration, $[V_{Mg}^{''}]$ is Mg-vacancy concentration, and the **a** terms are T dependent. Ideally we could distinguish the individual contributions of $Fe_{Mg}^{\bullet}$ and $V_{Mg}^{''}$ because they have individual concentration and mobility dependences on T. Realistically a simpler model of undifferentiated mixed conduction of $Fe_{Mg}^{\bullet}$ and $V_{Mg}^{''}$ best describes our data. $V_{Mg}^{''}$ are expected to have higher Ea than $Fe_{Mg}^{\bullet}$ [*Wanamaker and Duba*, 1993; *Hirsch and Shankland*, 1993], however our data indicate that for 1000ºC<T<1500ºC a single Ea can be used to calculate σ of olivine.

[9] The defect model is produced using a multivariable nonlinear least-squares fitting of σ data as a function of both T and fO_2. Data from the two [001] samples are in excellent agreement (Figure 1); a model of these two samples must have fit parameters that are also in agreement. Thermopower measurements

[*Schock et al.*, 1989; *Wanamaker*, 1994; *Constable and Roberts*, 1997] indicate that $Fe^{\bullet}_{Mg}$ conduction dominates over $V^{''}_{Mg}$ conduction below 1300 °C. Due to extrinsic defects common in olivine, such as Ca, we expect there to be a minimum σ that is not affected by fO_2 [*Constable and Roberts,* 1997; *Duba and Constable*, 1993], also at reducing fO_2 electronic conduction becomes significant [*Stocker,* 1978], explaining the slight curvature in our data at reducing fO_2. Combining these considerations yields our model:

$$\sigma = \{\sigma_0 fO_2^{S} + \sigma_{min}\}e^{-Ea/kT}. \quad (4)$$

$\boldsymbol{\sigma_0}$ is the pre-exponential conductivity term, which is dependent on $[Fe^{\bullet}_{Mg}]$ and $[V^{''}_{Mg}]$ and the entropies of their mobilities. $\boldsymbol{\sigma_{min}}$ is the non-specific fitting parameter to describe the slight curvature in our data. **S** is the stoichiometric coefficient describing the increase of intrinsic defect concentrations with fO_2. **Ea** is a combination of the formation (intrinsic) and hopping (intrinsic and extrinsic) energies of defects in olivine. **k** is the Boltzmann constant. Initial fitting with an adjustable S parameter favored S = 0.161-0.166 for all four samples (Table 1). Fixing S to the expected value of 2/11 [*Stocker*, 1978] yields excellent fits to the data; we use this constraint in our model.

[10] Fitting each data set to Equation 4 with fixed S = 2/11 led to excellent agreement between fits of the two [001] oriented samples, with each of the parameters overlapping in fitting error between fits (Table 1). A geometric mean of the fits from these two samples is used: $\sigma_{[001]} = \{\sigma_{[001]A}\sigma_{[001]B}\}^{1/2}$. Fits of SCC2_010A and SCC2_100B are used as $\sigma_{[010]}$ and $\sigma_{[100]}$ respectively. Fitting results (Figure 2, **bold** entries in Table 1) yield σ of self-buffered dry olivine as a function of orientation, T, and fO_2. Electronic conduction is not specifically included in the model but may be significant for fO_2 lower than our experimental range [*Stocker and Smyth,* 1978]. Also the effects of pyroxene buffering [*Wanamaker and Duba*, 1993] are not included in the model.

[11] The fO_2-independent $Ea_{[001]} > Ea_{[010]} > Ea_{[100]}$ are much smaller than those calculated using a constant $7CO_2$:1CO gas mixture and heating rate of 1ºC/min by *Schock et al.* [1989], in agreement with *Wanamaker and Duba* [1993]. The fitting errors for Ea are small (Table 1). $Ea_{[100]}$ = 0.33 eV compares reasonably to the value of 0.55 eV by *Wanamaker and Duba* [1993] and for calculations for polarons in olivine (~0.4 eV) by *Hirsch and Shankland* [1993]. Figure 2 shows the Arrhenius behavior of olivine anisotropy for fO_2 buffered by quartz-fayalite-magnetite (QFM). The azimuthal conductivity contrast of a dry [100]-oriented layer is small and would not be detectable for T near 1100ºC. The anisotropy of a dry [100]-oriented layer might be detectable at higher and lower T; the model indicates a 0.4 log unit contrast at 1500ºC. Different fO_2 buffers have a small affect on relative electrical anisotropy, and a larger affect on the absolute (and isotropic) values.

[12] A geometric mean of the 3 equations for each principal orientation describes the electrical conductivity of a self-buffered isotropic olivine medium in which the minor effects of grain size and boundaries [*Roberts and Tyburczy*, 1993; *Xu et al.*, 2000] are unaccounted for:

$$\sigma_{GM} = (\sigma_{[100]}\sigma_{[010]}\sigma_{[001]})^{1/3}. \quad (5)$$

Equation 5 can be simplified by ignoring cross-terms (Table 1 [*e.g., Constable et al.*, 1992]).

$$\sigma_{GM} \approx [2.51(S/m)\, fO_2^{2/11} + 0.0653(S/m)]e^{-0.531(eV)/kT}. \quad (6)$$

This equation is for fO_2 in atm and has a maximum difference of -0.00275 log units for σ calculated using Equation 5 or 6 between 727-1408ºC. This model allows us to examine the case of a dry isotropic olivine medium for a range of T and fO_2 buffering. Figure 3 shows σ_{GM} corresponding to QFM, NNO (Ni-NiO buffer), WM (wüstite-magnetite buffer) and a constant $7CO_2$:1CO gas mixture (for which SO1 and SO2 isotropic models are based).

DISCUSSION

[13] A mixed conduction model of $Fe_{Mg}^{\bullet}$ and $V_{Mg}^{''}$ successfully describes our carefully performed fully equilibrated σ measurements of olivine. We explore σ of an effective isotropic olivine medium as a function of fO_2 and T. For T<1300ºC and the fO_2 of a $7CO_2$:1CO gas mixture, σ_{GM} is higher in magnitude than the SO1 [*Shankland and* Duba, 1990] and SO2 [*Constable et al.*, 1992] models (Figure 3). The σ_{min} term that we required to describe the contributions of electrons and other defects dominates the σ extrapolation to low T and concurrent low fO_2 conditions, with σ ~0.6 log units higher in magnitude than the SO1 and SO2 models at T=1000ºC. The σ_{min} term is nonspecific but appropriately describes a flattening out of fO_2 dependence at low fO_2 (Figure1) [*Schock et al.*, 1989]. Explicit treatment of the nonlinear fO_2 dependence and fully equilibrated data causes the higher σ and lower apparent Ea. The model lacks defect specific information for T below 1000ºC where equilibrated σ and thermopower measurements of single crystal olivine are needed.

[14] The model indicates at the single-crystal scale the maximum azimuthal σ contrast is less than $10^{0.4}$ S/m or an anisotropy factor of ~2.5 for 1000ºC<T<1500ºC. Anisotropy factors of olivine-enstatite aggregates deformed by simple shear are expected to be significantly less than that of a single-crystal [*Simpson and Tommasi*, 2005]. This result supports the contention that another mechanism, such as enhanced conductivity and anisotropy due to the presence of water [*Simpson*, 2002; *Karato*, 1990], is necessary to explain upper mantle anisotropy observed by MT. For the lowest values of mantle anisotropy observed by MT the σ contribution of olivine's intrinsic defects may play a small role. The mixed conduction model can be modified to include a term that theoretically estimates the contribution of H^+ to olivine σ [*Karato*, 1990; *Simpson and Tommasi*, 2005] to predict electrical anisotropy at the single-crystal scale for water poor conditions. σ measurement of hydrated olivine would be invaluable in determining the source of electrical anisotropy in the mantle.

Acknowledgements. We thank Steve Constable and two anonymous reviewers for valuable comments and suggestions, Rick Ryerson and Gordon Moore for EPMA measurements, Tom Groy for XRD, Bill Ralph and Will Dalrymple for help with the experiments. Part of this work was performed under the auspices of the U.S. Department of Energy (DOE) by University of California, Lawrence Livermore National Laboratory (LLNL) under Contract W-7405-Eng-48. The project (04-LW-077) was funded by the Laboratory Directed Research and Development Program at LLNL. This work was also supported by NSF EAR 0073987 to Arizona State University (JAT).

REFERENCES

Constable S., and J. J. Roberts (1997), Simultaneous modeling of thermopower and electrical conduction in olivine, *Phys. Chem. Minerals*, 24, 319-325.

Constable S., T. J. Shankland, A. G. Duba (1992), The electrical conductivity of an isotropic olivine mantle, *J. Geophys. Res.*, 97, 3397-3404.

Duba A. G., S. Constable (1993), The electrical-conductivity of lherzolite, *J. Geophys. Res.*, 98, 11885 11899.

Eaton D. W., A. G. Jones, and I. J. Ferguson (2004), Lithospheric anisotropy structure inferred from collocated teleseismic and magnetotelluric observations: Great Slave Lake shear zone, northern Canada, *Geophys. Res. Lett.*, 31, L19614,doi:10.1029/2004GL020939.

Evans R. L., G. Hirth, K. Baba, D. Forstyh, A. Chave, and R. Mackie (2005), Geophysical evidence from the MELT area for compositional controls on oceanic plates, *Nature*, 437, 249-252.

Grove T. L. (1981), Use of FePt alloys to eliminate the iron loss problem in 1-atmosphere gas mixing experiments - theoretical and practical considerations, *Cont. Min. Pet*., 78(3), 298-304.

Hirsch L. M., and T.J. Shankland (1993), Quantitative olivine-defect chemical model: insights on electrical conduction, diffusion, and the role of Fe content, *Geophys. J. Int.*, 114, 21-35.

Hirsch L. M., T.J. Shankland, and A. G. Duba (1993), Electrical conduction and polaron mobility in Fe-bearing olivine, *Geophys. J. Int.*, 114, 36-44.

Huang X., Y. Xu, and S. Karato (2005), Water content in the transition zone from electrical conductivity of wadsleyite and ringwoodite, *Nature,* 434(7034), 746-749.

Karato S. (1990), The role of hydrogen in the electrical-conductivity of the upper mantle, *Nature*, 347(6290), 272-273.

Netherton R., and A. G. Duba (1978), An apparatus for simultaneously measuring electrical conductivity and oxygen fugacity, Lawrence Livermore National Laboratory Internal Document, UCRL-52394.

Nitsan U. (1974), Stability field of olivine with respect to oxidation and reduction, *J. Geophys. Res.*, 79, 706-711.

Roberts J. J., and J. A. Tyburczy (1991), Frequency dependent electrical properties of polycrystalline olivine compacts, *J. Geophys. Res.*, 96 (B10), 16205-16222.

Roberts J. J., and J. A. Tyburczy (1993), Impedance spectroscopy of single and polycrystalline olivine: evidence for grain boundary transport, *Phys. Chem. Minerals*, 20, 19-26.

Shankland T. J., and A. G. Duba (1990), Standard electrical conductivity of isotropic, homogenous olivine in the temperature range 1200˚-1500˚C, *Geophys. J. Int.*, 103, 25-31.

Schock R. N., A. G. Duba, and T. J. Shankland (1989), Electrical conduction in olivine, *J. Geophys. Res.*, 94, 5829-5839.

Simpson F. (2002), Intensity and direction of lattice-preferred orientation of olivine: are electrical and seismic anisotropies of the Australian mantle reconcilable?, *Earth Planet. Sci. Lett.*, 203, 535-547.

Simpson F., and A. Tommasi (2005), Hydrogen diffusivity and electrical anisotropy of a peridotite mantle, *Geophys. J. Int.*, 160, 1092-1102.

Stocker R. L., and D. M. Smyth (1978), Effect of enstatite activity and oxygen partial pressure on point-defect chemistry of olivine, *Phys. Earth Planet. Inter.*, 16, 145-156.

Stocker, R. (1978) Influence of oxygen pressure on defect concentrations in olivine with a fixed cationic ratio, *Phys. Earth Planet. Inter.*, 17, 118-129.

Wanamaker B. J. (1994), Point defect diffusivities in San Carlos olivine derived from reequilibration of electrical conductivity following changes in oxygen fugacity, *Geophys. Res. Lett.*, 21, 21-24.

Wanamaker B. J., and A. G. Duba (1993), Electrical conductivity of San Carlos olivine along [100] under oxygen- and pyroxene-buffered conditions and implications for defect equilibria, *J. Geophys. Res.*, 98, 489-500.

Xu Y., T. J. Shankland, and A. G. Duba (2000), Pressure effect on electrical conductivity of mantle olivine, *Phys. Earth Planet. Inter.*, 118, 149-161.

FIGURE 1: Fitted conductivity of single crystal SCO at a) 1100ºC, b) 1200ºC, and c) 1300ºC. Fits are summarized in Table 1. OST- and OST+ mark the olivine stability field [*Nitsan*, 1974]. *Schock et al.* [1989], and *Wanamaker and Duba*, [1993] are normalized to $Fo_{89.1}$ for comparison [*e.g. Hirsch et al.*, 1993]. Our 'SCC2' data is ~0.15 log units higher than previous data as a result of less Fe loss.

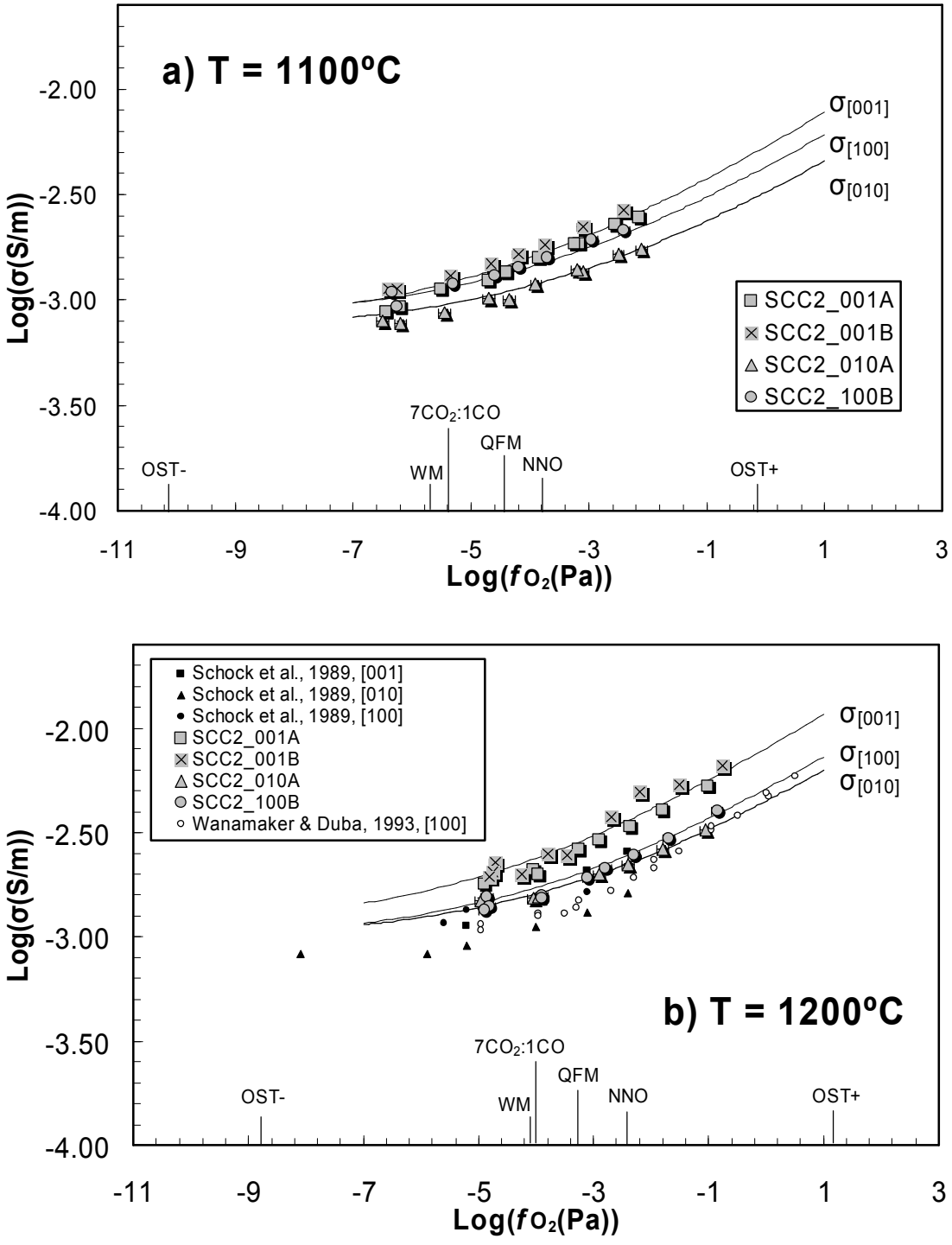

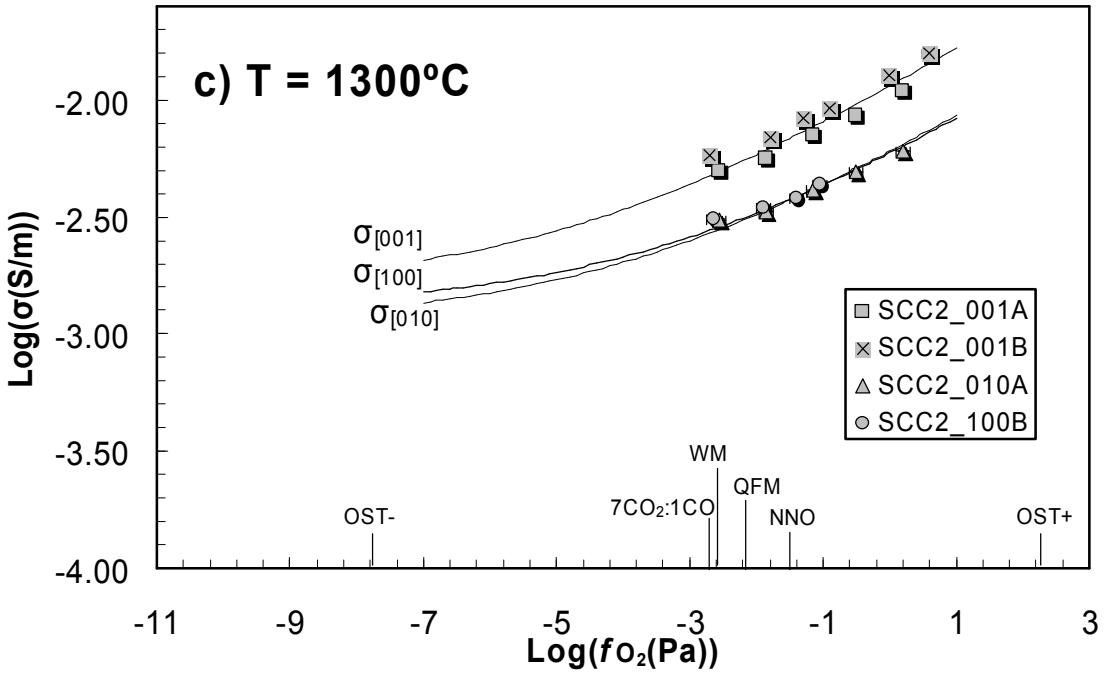
c) T = 1300ºC
-2.00
-2.50
-3.00
-3.50
-4.00
Log(σ(S/m))
σ[001]
σ[100]
σ[010]
SCC2_001A
SCC2_001B
SCC2_010A
SCC2_100B
WM
QFM
NNO
OST-
7CO2:1CO
OST+
-11
-9
-7
-5
-3
-1
1
3
Log(fO2(Pa))

Figure 2: Olivine anisotropy from our model for fO_2 from a QFM oxygen buffer. The three principal orientations are plotted for azimuthal comparison with a maximum σ contrast of ~$10^{0.4}$ S/m for this T range.

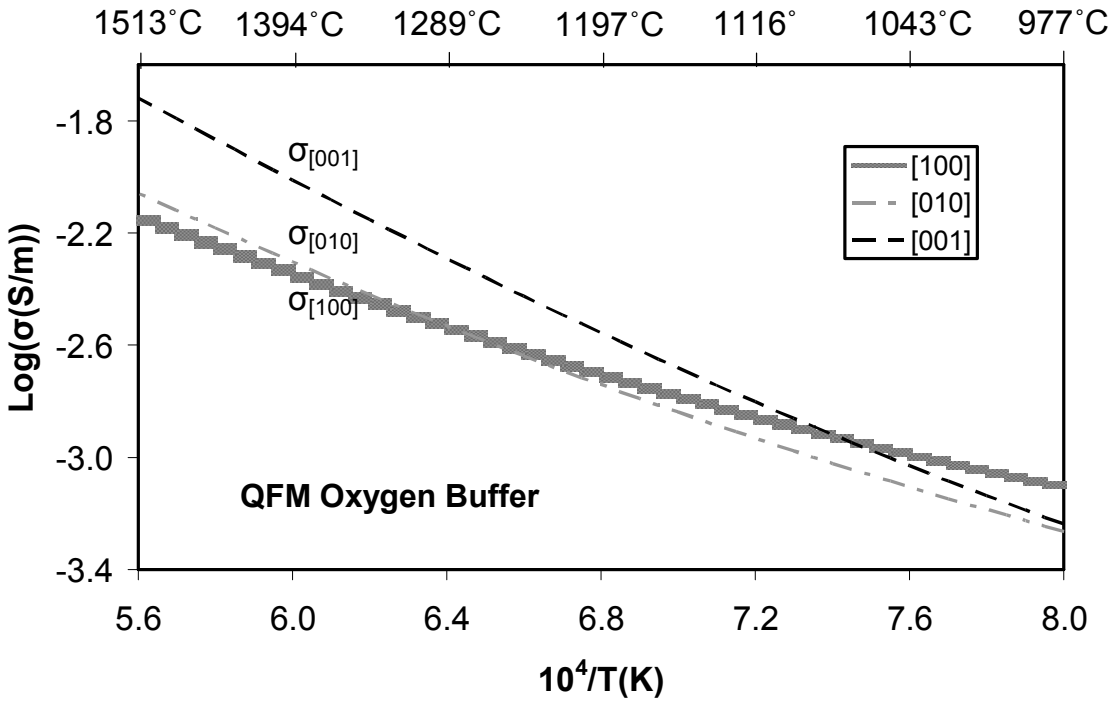

Figure 3: σ_{GM} from SCC2 model for a variety of fO_2 buffering: QFM, Ni-NiO (NNO), a $7CO_2$:1CO gas mixture, and wüstite-magnetite (WM). SO1 [*Shankland and* Duba, 1990], SO2 [*Constable et al.*, 1992], and the polycrystalline compact model by *Xu et al.* [2000] have each been normalized to $Fo_{89.1}$ [e.g. *Hirsch et al.*, 1993].

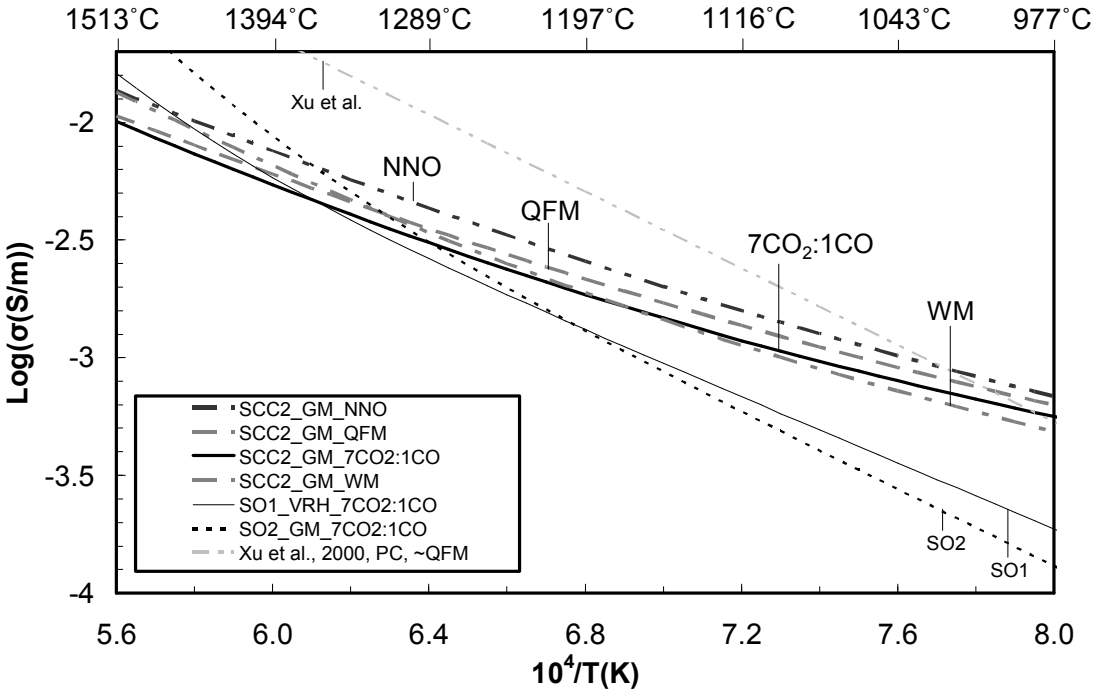

Table 1: Fitting parameters and error for each sample corresponding to Equation 4 for fO_2 in atm. The confidence intervals for the parameters are 99%. The errors are standard deviation estimates made by dividing fitted parameters by their respective t-ratios. Fits used in our model are in **bold** print.

SAMPLE	σ_0 (S/m)	σ_{min} (S/m)	S	Ea (eV)	R^2
SCC2_100B	0.362 +/- 0.125	0.00968 +/- 0.00451	0.161 +/- 0.014	0.326 +/- 0.046	0.991
SCC2_010A	1.92 +/- 0.25	0.0626 +/- 0.0110	0.161 +/- 0.006	0.558 +/- 0.017	0.999
SCC2_001A	10.5 +/- 1.5	0.163 +/- 0.041	0.166 +/- 0.006	0.695 +/- 0.041	0.999
SCC2_001B	14.9 +/- 4.5	0.268 +/- 0.114	0.161 +/- 0.017	0.720 +/- 0.029	0.996
[001] approx. mean	12.5 +/- 2.8	0.209 +/- 0.071	0.164 +/- 0.012	0.708 +/- 0.035	N/A
Geometric Mean	4.43 +/- 0.48	0.0502 +/- 0.0164	0.162 +/- 0.011	0.531 +/- 0.033	N/A
SCC2_100B	**0.432 +/- 0.147**	**0.0119 +/- 0.0051**	**Fixed 2/11**	**0.322 +/- 0.048**	**0.991**
SCC2_010A	**2.39 +/- 0.35**	**0.0798 +/- 0.0147**	**Fixed 2/11**	**0.561 +/- 0.021**	**0.998**
SCC2_001A	12.8 +/- 2.2	0.250 +/- 0.056	Fixed 2/11	0.696 +/- 0.025	0.998
SCC2_001B	18.3 +/- 3.8	0.343 +/ - 0.092	Fixed 2/11	0.724 +/- 0.029	0.996
[001] approx. mean	**15.3 +/- 2.9**	**0.293 +/- 0.072**	**Fixed 2/11**	**0.710 +/- 0.027**	**N/A**
Geometric Mean	**2.51 +/- 0.57**	**0.0653 +/- 0.0187**	**Fixed 2/11**	**0.531 +/- 0.032**	**N/A**